

Simulations of the glaciation of a frontal mixed-phase cloud with the Explicit Microphysics Model

By V. T. J. PHILLIPS¹, T. W. CHOULARTON^{1*}, A. J. ILLINGWORTH², R. J. HOGAN² and P. R. FIELD³

¹Physics Department UMIST, Manchester, UK

²Department of Meteorology, University of Reading, UK

³Met Research Flight, Met Office, UK

(Received 4 April 2002; revised 4 September 2002)

SUMMARY

Simulations with the Explicit Microphysics Model (EMM) of a case of lightly precipitating, glaciated stratiform cloud are presented. This frontal cloud was observed by the UK Met Office C-130 aircraft and the dual-polarization radar at Chilbolton in southern England.

The Hallett–Mossop (H-M) process was found to cause extremely high number concentrations of crystal columns of up to almost 1000 l^{-1} in the H-M region (-3 to -8°C) of the updraught in the EMM control simulation. Similarly high number concentrations of ice particles were seen in, and in the vicinity of, ascending thermals in the aircraft observations. Such concentrations are orders of magnitude higher than the ice nucleus (IN) concentration. Moreover, the dendritic growth of highly planar particles of primary ice produces a peak in differential reflectivity of almost 4 dB just below the cloud top (-15°C). Primary ice particles are generally larger than H-M splinters and mostly determine the simulated radar properties of the model cloud.

Tests with the EMM revealed significant sensitivities of the average ice number concentration, the cloud- and ice-water paths, and the surface precipitation rate, to atmospheric concentrations of IN and cloud condensation nuclei for this frontal-cloud case. The layer of supercooled cloud-water located just below cloud top in the control is depleted by evaporation when the IN concentration is augmented.

KEYWORDS: Differential reflectivity Hallett–Mossop process Ice crystal multiplication Stratiform

1. INTRODUCTION

An investigation into the nature of glaciation in mixed-phase stratiform layer cloud is presented. The glaciation in stratiform cloud is an important process on all scales for several reasons. The ice microphysics in such cloud is fundamental to the production of precipitation. Most of the surface precipitation in midlatitudes falls from frontal layer cloud. The Bergeron–Findeisen process (Rogers and Yau 1991) promotes the efficient formation of precipitation embryos in mixed-phase layer cloud. This mechanism involves the deposition onto ice crystals of vapour evaporated from cloud water. Also, the optical depth and effective particle radius influence the radiative properties of a cloud, depending on rates of nucleation and growth of ice crystals. Finally, the release of latent heat during glaciation has a marked effect on the dynamical evolution of layer cloud.

Bower *et al.* (1996) observed high number concentrations of ice crystals near the -6 and -15°C levels in extratropical frontal stratiform cloud. These number concentrations exceeded the expected concentrations of primary ice nuclei (IN) by orders of magnitude. The Hallett–Mossop (H-M) process of ice particle multiplication (Hallett and Mossop 1974) is one possible mechanism that has been proposed to account for such high crystal number concentrations. During the riming of large droplets onto ice particles, fragments of ice are seen to be emitted at temperatures within the range of -3 to -8°C in laboratory experiments.

The efficacy of the H-M process depends on the abundance of supercooled cloud-water. The low rate of ascent over most of the area of stratiform cloud is insufficient to support large cloud-water contents, because the low rate of supply of vapour to sub-zero

* Corresponding author: Department of Pure and Applied Physics, UMIST, PO Box 88, Manchester M60 1QD, UK. e-mail: t.w.choularton@umist.ac.uk

© Royal Meteorological Society, 2003. P. R. Field's contribution is Crown copyright.

levels does not maintain a supersaturation that is high enough for much condensation to occur. However, there are usually cells of convection embedded within stratiform layers. Ascent of cloudy air in these cells augments the supply of cloud-water for riming and H-M splinter production. Mixed-phase stratiform cloud is often characterized by high rates of production of snow from the aggregation of ice over long time-scales. Saunders and Hosseini (2000) have observed H-M splinter production at terminal velocities $>2 \text{ m s}^{-1}$; much less is known about the H-M process at the lower fall speeds corresponding to snowflakes.

In this study, a case of mixed-phase stratiform cloud over Chilbolton in the UK that was observed by aircraft and polarization-diversity radar (Hogan *et al.* 2002) is utilized for microphysical simulations with the Explicit Microphysics Model (EMM). This model includes a detailed representation of the H-M process and of the trajectories and growth of ice particles. Also, the model predicts some radar properties of the cloud for comparison with observations. Simulated radar properties include the differential reflectivity (Z_{DR}). This quantity increases monotonically with the non-sphericity, bulk density and degree of alignment of the scattering particles.

The overall aim for the microphysical modelling in the present paper is: (i) to define a dynamical environment which is a realistic representation of what was observed; (ii) to examine whether certain combinations of microphysical processes acting within this dynamical framework are capable of reproducing some of the key microphysical characteristics as observed by aircraft and dual-polarization radar; and (iii) to outline the salient dependencies of the mixed-phase microphysics on important characteristics of the large-scale environment.

In section 2 there is a brief description of the EMM; sources of more detailed information about the model are referred to. The selection of values for input parameters in the model is presented and details of the observed case outlined in section 3. The results from the control simulation are described and compared with observations in section 4. In section 5, the results from sensitivity tests are provided. The conclusions are presented and discussed in section 6.

2. THE MODEL

The EMM developed by Phillips (2001) is an extension to the one-dimensional (1D) Multi-Thermal Model of cumulus glaciation by Blyth and Latham (1997). Fully interactive components for vapour, cloud-water and rain, as well as aggregation of ice, heterogeneous and homogeneous freezing, melting, simulated radar properties and the evolution of crystal shape (or ‘habit’) during particle growth are some of the new processes incorporated into the EMM by Phillips (2001).

A detailed representation of the cloud dynamics is prescribed as an input for the prediction by the EMM of the microphysical development of the cloud. For the present study, the EMM has been further modified to incorporate a representation of the surrounding cloudy region (SCR) of weak ascent outside the single updraught. Thermals ascend at regular intervals through the updraught. Their ascent rate is a prescribed fraction (50%) of a reference value of maximum vertical air velocity in the interior of the cloud. This reference velocity displays a linear increase with height from a value w_{cb} at cloud base, to a value w_{max} at a level z_{max} at upper levels. It decreases linearly with height from $z = z_{max}$ towards cloud top. From the ascent rate of thermals, the actual peak updraught strength is inferred with formulae for a spherical vortex (see Levine 1959). As thermals ascend, their expansion by pressure loss and entrainment, and their horizontal drift according to the vertical wind shear, are evaluated. The horizontal drift

of thermals determines the updraught slope. Thermals entrain ice and cloud-water from the SCR. There is a uniform prescribed value for the ascent rate of air throughout the SCR.

The evolution of the size distribution of liquid and ice particles is explicitly predicted at each level in the updraught and SCR by the EMM. The size distribution is discretized with size categories that form a variable grid. Trajectories of ice particles are traced on the vertical (x, z) plane coinciding with the updraught by applying a prescribed 2D field of air velocity (u, w):

$$DX_c/dt = u(x, z, t), \quad (1)$$

$$dZ_c/dt = w(x, z, t) - v_t(R). \quad (2)$$

Each category has a position (x_c, z_c) on the (x, z) plane and occupies a shallow layer of either the updraught or SCR. The terminal velocity, v_t , of particles in a category is determined in the manner presented by Pruppacher and Klett (1997) for cylindrical and spheroidal shaped particles for predicted values of size, bulk density and axial ratio. Particles in a given category are uniformly distributed throughout the category volume.

There appears to be no observational evidence that supercooled raindrops were present in the images obtained from the 2D imaging cloud and precipitation particle probes (2D-C and 2D-P) for the particular glaciated stratocumulus case at Chilbolton simulated in this paper (see subsection 3(a) and Hogan *et al.* (2002)). Consequently, raindrop production by coalescence is prohibited here, in contrast with previous EMM simulations of glaciated cumuli.

Condensational growth and advection for cloud-water are represented by the tracing of trajectories of categories of droplets and vapour in 1D. Size categories of droplets are formed by primary nucleation at the cloud base. They may also be initiated by secondary droplet nucleation at any level in the cloud when the supersaturation begins to exceed the cloud-base value (see Rogers and Yau 1991). Secondary droplet nucleation is the process that ‘spins up’ the cloud-water content from zero throughout the model cloud at $t = 0$. A power-law activity spectrum for cloud condensation nuclei (CCN) is assumed for the nucleation of droplets:

$$N_w = Cs^k. \quad (3)$$

Here, N_w is the number concentration of CCN activated at supersaturations less than s (%), while C and k are constants. Hence, when cloud-water is evaporated away by the Bergeron–Findeisen process, new droplets may later be supplied by secondary droplet nucleation.

Number concentrations of droplet categories at a given level of the updraught are normalized at each time-step according to the equation for the evolution of their total mixing ratio of cloud-water:

$$dQ_w/dt = 3(\mu_E/R_{th})w_{th}(Q_{w,SCR} - Q_w) + T. \quad (4)$$

Here, T is the condensation/evaporation source of cloud-water obtained by tracing the trajectories of categories of droplets and vapour along the axis of the updraught or SCR. The velocity scale for the local rate of ascent of thermals is denoted by w_{th} and the radius of thermals is R_{th} . The subscript SCR refers to the corresponding value in the SCR for a given level. There is a similar equation for the evolution of the vapour mixing ratio in the updraught:

$$dQ_v/dt = 3(\mu_E/R_{th})w_{th}(Q_{v,SCR} - Q_v) - T. \quad (5)$$

Similar equations to (4) and (5) are applied for cloud-water growth and advection in the SCR, except that the entrainment term is omitted. The fractional entrainment

rate (s^{-1}) of thermals is represented by the factor, $3(\mu_E/R_{\text{th}})w_{\text{th}}$, where μ_E is a dimensionless entrainment constant. For laboratory thermals that are self-similar in an un-sheared environment, experimental studies indicate that $\mu_E \sim 0.25$ (Sanchez *et al.* 1989). Self-similarity is attained when a thermal has propagated a distance that is at least about four times its initial diameter.

Thermals arriving at most levels in the cloud are likely to have already propagated by several times their initial depth, if their initial size is very much less than the cloud depth. This condition is satisfied in the case simulated here (see section 3). It is also assumed that thermals originate from near, or below, the cloud base. Hence, thermals in the model are assumed to be self-similar. (In some circumstances a thermal in the real cloud might originate from a layer above the cloud base if that layer becomes the first to become unstable during lifting; this possibility is neglected in the model.)

Primary ice nucleation is represented with a version of the formula for condensation-freezing/deposition given by Meyers *et al.* (1992). The original version of this formula is multiplied everywhere by a prescribed constant, Ψ , in the EMM since the IN concentration in the real atmosphere can differ widely from the formula of Meyers *et al.* The process of H-M ice multiplication is represented with inclusion of the observed dependence on temperature and on the size of large droplets seen in laboratory studies (Pruppacher and Klett 1997); supercooled droplets between -3 and -8 °C must be larger than about $24 \mu\text{m}$ for H-M splinters to be emitted on impact with the ice surface. Moreover, it is hypothesized in the present study that any type of ice particle is capable of H-M splinter production if it is sufficiently large to rime (see section 1). Moreover, it is assumed that the droplet-size dependence of this rime-splintering is the same for snow as for graupel.

Accretion of ice and supercooled cloud-water by an ice particle of mass, m_R , and radius, R , is represented as a continuous collection process:

$$dm_R/dt = \int_0^R A(R, r)E_c(R, r)\{v_t(R) - v_{t,y}(r)m_y N_y(r)\} dr. \quad (6)$$

Here, m_y is the mass of the collected particle of radius, r , and of the y th species, having a number density, $N_y(r)$, and a terminal velocity, $v_{t,y}(r)$. The collection efficiency is $E_c(R, r)$, and the area for sweep-out is $A(R, r)$ (see Rogers and Yau 1991). The density of new layers of accreted ice from the application of Eq. (6) are given a fixed value of 100 kg m^{-3} , which is at the centre of the range of values for the bulk density of snowflakes provided by Pruppacher and Klett (1997). Large, quasi-spherical aggregates $>1 \text{ mm}$ of density 100 kg m^{-3} are generated from collisions between snow particles $<1 \text{ mm}$ with a scheme based on the autoconversion algorithm by Murakami (1990), see also Reisner *et al.* (1998). Explicit predictions of the mean and standard deviation of the terminal velocity, and of the mean number concentration and geometric cross-sectional area of such snow particles, are utilized in this scheme. Sticking efficiencies for aggregation are derived from data provided by Mitchell (1988) and are applied for this scheme and for continuous accretion of ice (see Eq. (6)).

Ice particles are represented as either cylindrical or spheroidal hydrometeors of variable axial ratio, $AR(t)$:

$$AR \equiv h_i/d_i. \quad (7)$$

Here, h_i and d_i are the length and diameter of the particle parallel and perpendicular to its axis of revolution. A planar ($AR < 1$) or columnar ($AR > 1$) shape will develop according to the ambient temperature regime and intensity of accretion, as AR evolves during growth along the particle trajectory. Empirical relations are applied for the shape

and density of each new layer of ice on the particle during growth by vapour deposition, riming and aggregation:

$$\delta h_i / \delta d_i \approx \chi_I, \quad (8)$$

$$\delta m_i / \delta V_i (\delta h_i, \delta d_i) \approx \rho_I. \quad (9)$$

Here, δm_i and δV_i are the mass and volume of the new layer of ice, which has thicknesses δh_i and δd_i in directions parallel and perpendicular to the particle axis during time-step δt . For vapour deposition, the empirical relations, $\chi_I = \chi_I(T, s)$ and $\rho_I = \rho_I(h_i, d_i, T)$, are derived from laboratory data presented by Pruppacher and Klett (1997). For riming and aggregation, χ_I is assigned prescribed values of 1/7 and 7 for $AR > 1$ and $AR < 1$ respectively. Consequently, AR naturally tends towards unity during intense accretion. Empirical formulae for the density of accreted rime in the EMM are documented by Phillips *et al.* (2001, 2002).

Equations (8) and (9) are solved iteratively, yielding values of δh_i and δd_i for each new layer of ice in δt . The bulk density of an ice particle is defined as m_i/V_i , where m_i and V_i are its total mass and volume. Planar and columnar particles are assumed to fall with their axes of revolution being vertical and horizontal respectively. Columns are assumed to be randomly oriented in the horizontal plane. When an ice particle finally falls out through the freezing level, its heat budget is solved to obtain the rate of melting. Eventually it is converted to a raindrop. Trajectories of rain categories are traced from the level of melting to the cloud base, where the precipitation rate is evaluated.

In summary: the model explicitly predicts the continuous evolution of the shape of identical particles in each size category following their motion through different regimes of temperature and accretion. From laboratory studies, it is well known that plates will tend to grow as columns in columnar regimes or as dendrites in dendritic regimes; columns will begin growing in a planar fashion after entering plate regimes. In real clouds, as in the EMM, the shape of a crystal is not generally fixed for its entire lifetime by the temperature regime of its nucleation (see Rogers and Yau 1991).

The total value and individual intrinsic components of the differential reflectivity are evaluated from the predicted shapes and bulk densities of particles in the simulated size spectra. The differential reflectivity is defined as:

$$Z_{DR} = 10 \log_{10}(Z_H/Z_V), \quad (10)$$

where Z_H and Z_V are the horizontal and vertical reflectivity factors. Z_{DR} is essentially a measure of the extent to which AR deviates from unity; it also tends to increase with the bulk density. Hogan *et al.* (2002) describe how the value of Z_{DR} varies with AR and bulk density, and explain how it may be calculated for particles which are aligned in the horizontal but have a random azimuthal orientation (see also Ryzhkov *et al.* 1998). For implementation in the EMM, Z_H and Z_V have been expressed in terms of the volume, V , of individual particles in the manner of Bader *et al.* (1987). Further details about the EMM are provided by Phillips (2001) and Phillips *et al.* (2001, 2002).

3. REALISTIC DEFINITION OF CLOUD DYNAMICS AND ENVIRONMENT FOR THE MODEL

(a) *Synopsis of observations*

The case simulated by the EMM control simulation comprises a lightly precipitating stratiform cloud observed near a warm front by the 3 GHz polarization-diversity radar at Chilbolton in England on 30 March 1999 (see Hogan *et al.* 2002). *In situ* measurements were made at 1214–1244 UTC by the UK Met Office C-130 aircraft. During this time

period, Lagrangian figure-of-eight patterns were flown between the -5 and -11 °C levels following a region of embedded convection that was being advected towards the north-east. The aircraft sounding shows that cloud top was near the -15 °C level, which corresponds to an altitude* of about 4.3 km. The cloud base is located at about 1 km, not far below the freezing level at 1.8 km.

The radar velocity data indicate a uniform vertical shear of the horizontal wind of $5 \text{ m s}^{-1} \text{ km}^{-1}$ for this case. Maxima in reflectivity, Z , above the freezing level were seen to be advected by a mean flow with an average horizontal velocity of about 1 km minute^{-1} . Such Z maxima ascended through the frontal cloud as maxima of vertical air velocity inside thermals. These vertically elongated ‘turrets’ were about 1 km in size. The intensity of the bright band at 1.8 km suggests that the high- Z values seen in thermals at sub-zero levels were caused by the presence of low-density, aggregated snowflakes.

The C-130 aircraft measured vertical air velocities with peak values of $1\text{--}2 \text{ m s}^{-1}$. The Particle Measuring System (PMS) probes on the aircraft were the Forward Scattering Spectrometer Probe (FSSP), and the 2D-C and 2D-P probes. The FSSP probe provided only an approximate estimate of the droplet number concentration since overcounting of droplets may occur when large ice particles are present (see Gardiner and Hallett 1985). Large number concentrations of small ice crystals were observed with these probes in and above the turrets. Supercooled cloud-water and rimed ice particles were observed in the turrets, reflecting the possibility of an active H-M process.

There was a general absence of supercooled raindrops in the 2D-C and 2D-P images, which is consistent with the assumption that coalescence was not a major mechanism for precipitation formation in this particular cloud (see section 2). The evident lack of coalescence in the real cloud is probably due to: (i) the proximity of the cloud base to the freezing level, allowing most of the depth of the cloud to be glaciated; and (ii) the low rate of ascent, with peak values of only $1\text{--}2 \text{ m s}^{-1}$, which promotes the evaporation of droplets by the Bergeron–Findeisen mechanism.

The area surrounding the turrets was seen to consist of: (i) one or two slanted streaks of high- Z_{DR} of about 3 dB, in which large number concentrations of pristine columns ($AR = 5$) were observed *in situ*; (ii) ubiquitous low- Z_{DR} values later on, owing to the presence of large quasi-spherical aggregates. Radar data only yield information about the largest particles present in a given region (Rogers and Yau 1991). The aggregates are also expected to have depleted the pristine columns by aggregation. Near cloud top, plumes of very high- Z_{DR} of up to 7 dB were seen to spread out into horizontal layers due to the growth of planar crystals; columnar crystals can never attain values higher than 4 dB.

The UK Met Office analysis for 1200 UTC on this day is presented by Hogan *et al.* (2002). The low-level isobars near the cold front are to the south of two cyclonic minima in pressure, and their orientation suggests that the geostrophic component of the low-level flow is south-westerly. The mean wind observed by the aircraft was from the 215° direction. Although no *in situ* observations of the CCN concentration were made at Chilbolton, the synoptic observations suggest that the airmass sampled in this observed case was probably maritime.

(b) *Input parameters matched to observed values*

The spatial extent and dynamics of the model cloud were prescribed according to observed values (see subsection 3(a)). The cloud-base level was set at 1.1 km (about

* Altitudes are given above mean sea level unless stated otherwise.

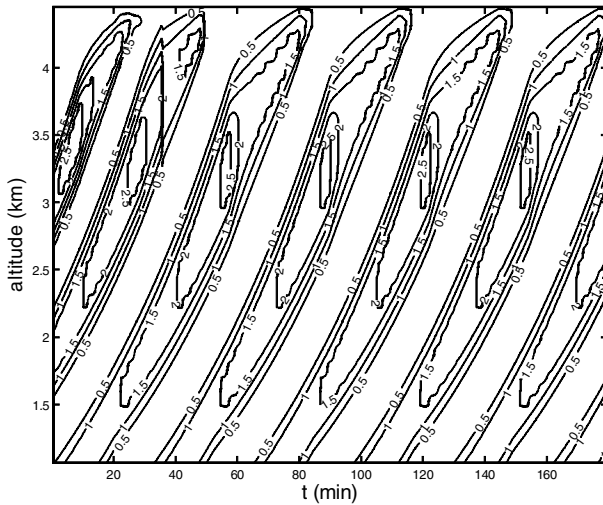


Figure 1. A height–time map of the evolution of the peak vertical air velocity (m s^{-1}) in the updraught of the Explicit Microphysics Model.

4°C). Figure 1 shows the evolution of the peak value of updraught strength at all levels. The reference profile of maximum vertical air velocity was prescribed ($w_{\text{cb}} = 1.0$; $w_{\text{max}} = 2.5$; $z_{\text{max}} = 4$ km) such that the actual peak updraught strength increased from about 1 m s^{-1} at cloud base to a maximum of about 2 m s^{-1} in the vicinity of 3.5 km in the EMM control simulation. The observed value of the vertical shear was applied in the control. An average updraught slope of 11 km of horizontal displacement for each 1 km of ascent between the freezing level and 4 km was produced by these choices of updraught strength and vertical wind shear. (The rate of ascent of thermals increases from $w_{\text{cb}}/2$ at cloud base to $w_{\text{max}}/2$ at 4 km.) At cloud base, thermals were initialized with a width and depth of 0.3 and 0.8 km respectively throughout the simulation. Their vertical spacing at cloud base was set at 0.4 km.

The vertical velocity in the SCR and debris regions of the updraught was somewhat arbitrarily assigned a value of 0.04 m s^{-1} , in the absence of precise aircraft observations of this quantity. Although the vertical air velocity in the SCR is almost negligible compared to the terminal velocity of ice, this ascent rate determines the vertical supply of vapour for condensation. Hence, it appears to be a sensitive parameter governing the profiles of cloud-water content. The width of the SCR was prescribed at 10 km and has the same slope as the updraught. The sloped axis of the SCR coincides with that of the updraught and the updraught is embedded inside the SCR. A value for the dimensionless entrainment constant of $\beta_E = 0.5$ was applied, causing the updraught width to increase with altitude from 0.3 km at cloud base to about 1.5 km near cloud top.

In the CCN activity spectrum the constants C and k were given values of 150 cm^{-3} and 0.5 respectively, which are standard values in the literature for maritime North Atlantic air (Hoppel *et al.* 1990). Observational studies of environmental IN concentrations appear to be fairly sparse in the literature. In the real atmosphere, IN concentrations are observed to be highly weather-dependent, and vary from day to day in an almost logarithmic fashion (Schnell *et al.* 1980; Hussain and Saunders 1984). Hence, the precise value of the IN concentration for the real cloud observed at Chilbolton on 30 March 1999 may not be inferred from the formula for deposition–condensation freezing provided by Meyers *et al.* (1992). This formula for the IN concentration includes no

dependence on the origin and history of the air mass. The individual values of the IN concentrations in the data collated by Meyers *et al.* (1992, see their Fig. 3) vary by only about one order of magnitude at any given temperature, partly because many of these original data were selected in order to minimize the air mass variability (Al-Naimi and Saunders 1985). Furthermore, Hussain and Saunders (1984) report that especially high IN concentrations are typically observed near the passage of a warm front. The stratiform cloud simulated here by the EMM is indeed warm-frontal. Consequently, the prescribed factor multiplying the formula from Meyers *et al.* (1992) for the IN concentration in this particular stratiform cloud has been assigned an arbitrary value of Ψ higher than unity ($\Psi = 3$), in the absence of any direct *in situ* observations.

4. NUMERICAL RESULTS FROM THE EMM CONTROL SIMULATION

Details of the EMM control simulation of this case are presented and explained here. Various predicted quantities are compared with the aircraft and radar observations documented by Hogan *et al.* (2002). Predictions of the number concentration of a microphysical species are regarded as satisfactory here if they are of the correct order of magnitude (see section 6). Time-averaged quantities for vertical profiles in the updraught are taken only from thermals. The duration of the simulation is 3 hours, of which the first 90 minutes are omitted in the standard time-averaging applied for all vertical profiles. This allows the model microphysics to approach a representative dynamical equilibrium before time-averaging begins. Average profiles of mean crystal properties (i.e. size, bulk density, AR) are derived by: (i) taking the mean over the number of particles in a given volume of the cloud at each time; and then (ii) performing the standard time-averaging for that volume at the end of the simulation. The H-M region is located between about 2.4 and 3.2 km altitude (-3 to -8 °C) in the model.

The average rate of surface precipitation in the control simulation is 0.5 mm hr^{-1} . The corresponding radar-observed value is of the order of magnitude of 1 mm hr^{-1} . The predicted average value of the cloud-droplet number concentration is about 20 cm^{-3} in the updraught and $<10 \text{ cm}^{-3}$ in the SCR, which agrees well with the observations (see subsection 3(b) and Hogan *et al.* (2002)). Also, the predicted average value of the droplet diameter is in the range 20 to 25 μm over most of the depth of the updraught (i.e. in thermals), and has similar values in the SCR. The mean droplet size in the H-M region is sufficient to allow H-M splinter production to be active throughout the model cloud. The EMM represents the droplet-size dependence of the H-M process seen in laboratory studies: droplets $>24 \mu\text{m}$ must be present for H-M multiplication to occur.

As is seen in the observations (Hogan *et al.* (2002), their Fig. 5), thermals comprising the updraught are predicted to be radar-visible as they comprise regions of high Z_H ascending through a low- Z_H supersaturated environment. Z_H has average predicted values in the range 15 to 20 dB(Z) in thermals and -5 to 5 dB(Z) in the SCR at most sub-zero levels. These high values of Z_H in the updraught are due to large, rimed aggregates in the model. In the 3 GHz radar observations for this case, thermals appear as vertically elongated regions also of about 20 dB(Z).

Figure 2 depicts the profiles of average Z_{DR} . Primary ice invariably determines the total Z_{DR} signal throughout the model cloud. The updraught is predicted to be a region of total $Z_{DR} \sim 0$ dB at sub-zero levels, because the large size of quasi-spherical aggregates ($AR \sim 1$) of primary ice causes these particles to dominate Z_H and Z_V . The component of intrinsic Z_{DR} of the relatively small H-M columns is larger but 'radar-invisible' in the model. (The 'intrinsic value' of Z_{DR} for particles in a certain species merely refers to the Z_{DR} that they would have if no particles in any other species were

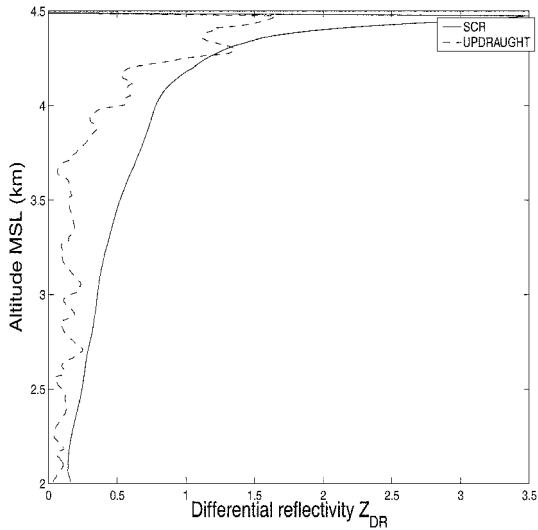


Figure 2. The differential reflectivity in the updraught and surrounding cloudy region (SCR).

present.) It is masked by the component associated with large primary aggregates. The radar-observed value of Z_{DR} in thermals was also practically zero (Hogan *et al.* 2002). The threshold for detection of significant positive Z_{DR} is assumed to be about 0.2 dB. Significantly positive Z_{DR} is predicted at almost all sub-zero levels in the SCR, as seen in the radar observations, owing to large primary aggregates being less numerous there than in the updraught. During the fallout of ice in the SCR, both accretion of ice and riming combine to restore the axial ratio of particles towards unity and to reduce the average bulk density. Hence, Z_{DR} decreases with decreasing altitude at most sub-zero levels in the SCR.

Figure 3 reveals the intrinsic components of Z_{DR} in the SCR predicted in the model. Above 4 km, values of $Z_{DR} > 1$ dB are found in the SCR. There is a peak of Z_{DR} in the range of 3 to 4 dB near the -15°C level at cloud top in the simulation. Similarly, the radar observations show horizontal layers of $1 < Z_{DR} < 7$ dB at levels near the cloud top above 4 km, in regions remote from ascending turrets. The peak near cloud top in the simulation is due to primary crystals growing in the dendritic regime. These dendrites grow realistically with a very low value of the axial ratio. The radar-invisible component of intrinsic Z_{DR} from H-M splinters has a time-averaged value of up to 0.5 dB in the SCR, exceeding the radar-visible Z_{DR} component of the larger primary crystals at most levels in and below the H-M region. The instantaneous value (not shown) of intrinsic Z_{DR} from H-M splinters reaches up to about 2 dB in fallstreaks in the SCR.

The maximum predicted value of the average intrinsic Z_{DR} for H-M columns is found to be about 3 dB lower than the corresponding maximum for primary ice in the control. This reflects the fact that the Z_{DR} of columnar crystals can never attain values > 4 dB whereas the Z_{DR} of planar crystals can attain much higher values of up to 10 dB (Hogan *et al.* 2002). H-M splinters are invariably columnar whereas the primary crystals are usually planar in the simulation. Columns may be oriented in all directions on the horizontal plane, which acts to reduce their apparent axial ratio.

Figure 4 displays the predicted profiles of the time-averaged number concentration of ice particles. At most sub-zero levels, the average number concentration of secondary

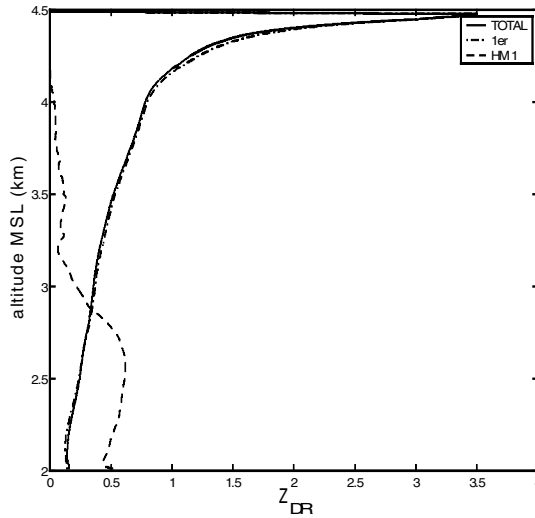


Figure 3. The vertical profile from the surrounding cloud region of intrinsic differential reflectivity, plotted as components for primary ice (dot-dashed line) and Hallett–Mossop splinters (dashed line), together with the total value (full line), at sub-zero levels.

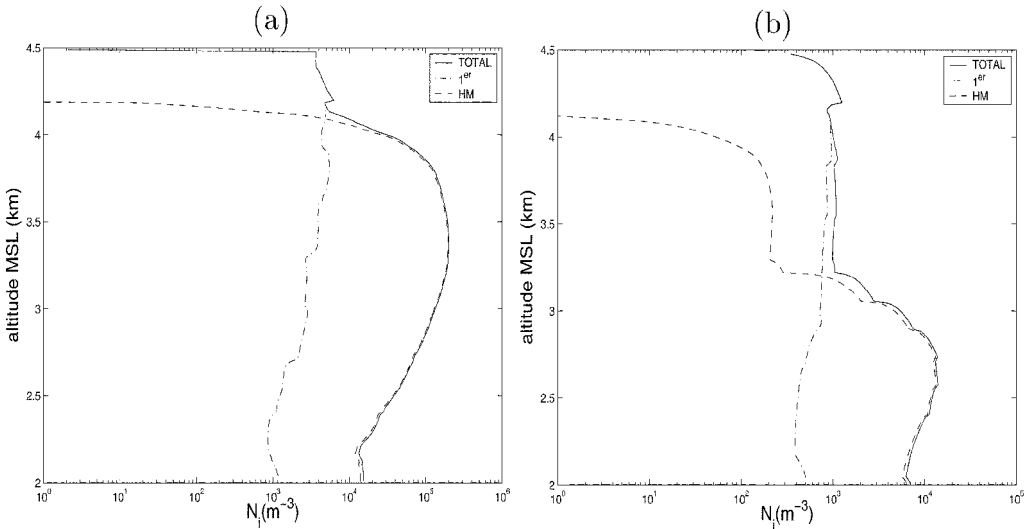


Figure 4. The ice number concentration in: (a) the updraught, and (b) the surrounding cloudy region, plotted as components for primary ice (dot-dashed line) and Hallett–Mossop splinters (dashed line), together with the total value (full line), at sub-zero levels.

ice is between one and two orders of magnitude greater than that of primary ice. A broad peak in the average ice number concentration of about 200 l^{-1} is predicted in the updraught at the top of the H-M region at 3.2 km ($-8 \text{ }^\circ\text{C}$). This peak is caused by H-M splinter production, and is two orders of magnitude higher than the predicted average value of the number concentration of primary ice. Most of these H-M splinters grow to become too large to be supported by the ascent of the updraught, falling out through the base of thermals into the SCR before reaching the cloud top. Non-negligible production of H-M splinters is also found in the SCR. Here, number concentrations of H-M splinters

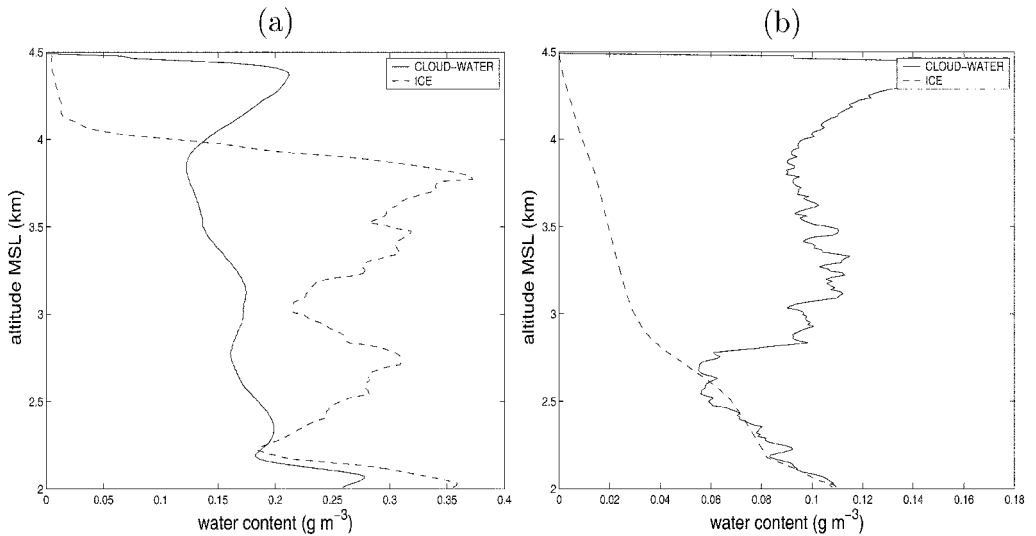


Figure 5. The vertical profiles of liquid- and ice-water contents in: (a) the updraught, and (b) the surrounding cloudy region.

only exceed those of primary ice below the top of the H-M region, since no ice can be upwelled in the SCR.

Maximum instantaneous values of the ice particle number concentration can be much higher than the time-averaged values displayed in the vertical profiles here. The highest instantaneous value of the total ice number concentration is predicted to be 900 l^{-1} over the width of the model updraught at -6°C due to a burst of H-M splinter production. At this level, the temperature-dependence of the H-M process optimizes the splinter production rate in the model. This maximum instantaneous value in the simulation may be compared with an observed maximum value of more than 1000 l^{-1} seen in the updraught at -6°C in the combined particle concentration data measured by the 2D-C and 2D-P probes on the aircraft (Hogan *et al.* (2002), their Fig. 7(c)). Such high values are two to three orders of magnitude higher than the average number concentration of primary crystals near cloud top in the updraught of the EMM control. It is possible that this observed maximum value may have been biased somewhat from contamination of the 2D-C probe by large droplets. However, further confirmation of the presence of large number concentrations of secondary ice particles in this real updraught at -6°C is evident from the observation of a simultaneous coincident peak of about 40 l^{-1} in the component of the 2D-C/2D-P concentration data filtered for particles $>150 \mu\text{m}$. In the model, the H-M splinters in this burst are very small, owing to competition for available vapour, and are predicted to be radar-invisible in the Z and Z_{DR} snapshots.

Figure 5 displays the predicted profiles of cloud- and ice-water contents in the updraught and SCR. The predicted values are all of order of magnitude 0.1 g m^{-3} at most sub-zero levels (compare with Hogan *et al.* (2002), their Figs. 4(c), 4(d) and 7(b)). The contribution from H-M splinters to the total ice-water content in the model is comparable with that from primary ice below 3 km in the SCR and also at most sub-zero levels in the updraught. The low value of the vertical air velocity in the SCR means that much of the vapour for deposition onto crystals must be provided by the evaporation of

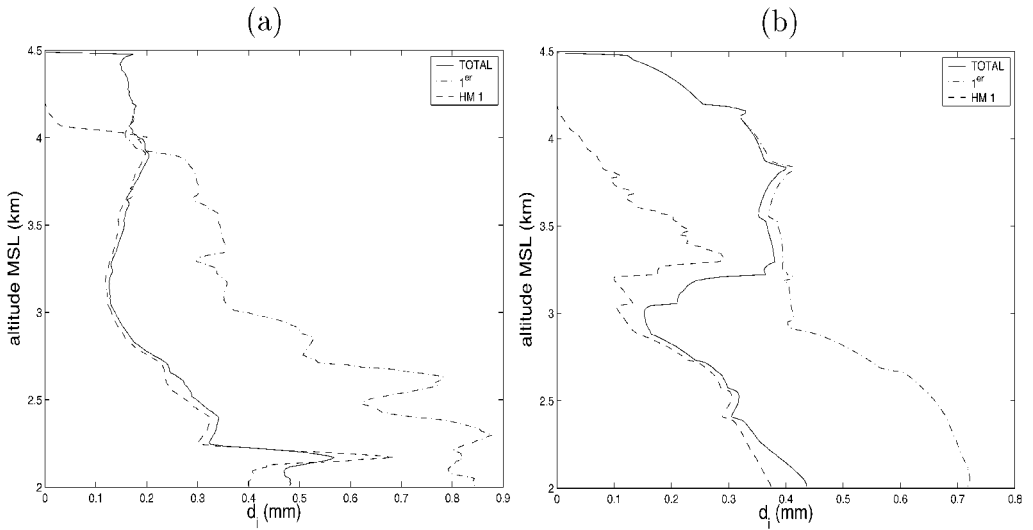


Figure 6. The time-averaged profile of the mean axial length of ice particles in: (a) the updraught, and (b) the surrounding cloudy region, plotted as components for primary ice (dot-dashed line) and Hallett–Mossop splinters (dashed line), together with the total value (full line), at sub-zero levels. For a given particle, the mean axial length is defined as half of the sum of the length and width of the particle.

cloud-water (i.e. by the Bergeron–Findeisen process). Partly for this reason, the cloud-water content is almost 50% lower in the SCR than in the updraught at most sub-zero levels in both the model and observations.

Cloud-water is present almost everywhere in the model cloud, mostly maintaining the vapour pressure close to the value for water saturation. This promotes the Bergeron–Findeisen process for development of precipitation embryos. A peak in the average cloud-water content of $\sim 0.2 \text{ g m}^{-3}$ is predicted in the highest 200 m layer just below the cloud top in the SCR and updraught of the simulation. This peak is related to low rates of loss of vapour from deposition onto young small crystals of primary ice, which causes a high supersaturation in the model.

The EMM explicitly predicts the continuous transition in particle size, bulk density and shape during accretion and motion of ice particles through different temperature regimes for vapour growth. Rapid growth of dendritic crystals in the SCR near the cloud top above 3.9 km (-12°C) is evident in Fig. 6. The average value of the mean ice diameter is greater for primary ice than for H–M splinters, typically by about 100%, at all sub-zero levels in the updraught and SCR. Good agreement is seen between the predicted value of the mean ice diameter and observed values of 2DC/2DP median volume diameter (Hogan *et al.* (2002), see their Figs. 7(d) and 9(d)). At -9°C the aircraft penetrated a turret, and observed values of 2DC/2DP median volume diameter, D_0 , of 0.25 mm were measured where the ice number concentration was about 50 l^{-1} ; at -6°C a value of D_0 of about 0.1 mm was observed in the updraught. Ice particles nucleated in the updraught fall into the SCR as lightly rimed crystals in the range of about 0.1 to 0.5 mm in size. The greater average size of primary crystals at all levels, relative to H–M splinters, is due to rates of primary nucleation being highest at the low temperatures near cloud top that favour rapid vapour growth (about -15°C ; see Rogers and Yau 1991).

Figure 7 depicts the time-averaged profiles of predicted mean bulk density of ice particles in the control simulation. (The largest, low-density aggregates do not

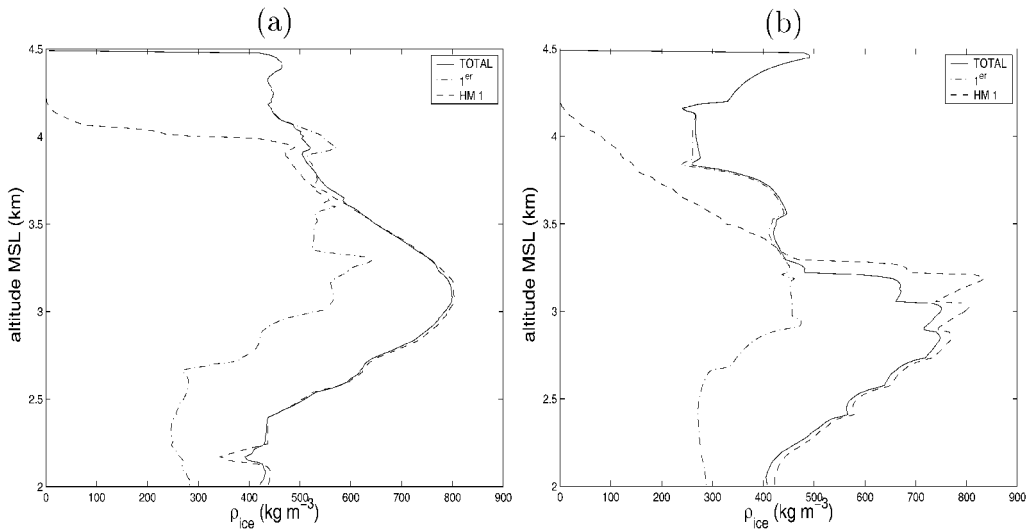


Figure 7. Same as Fig. 6 but for the mean bulk density (defined in section 2) of ice particles.

contribute appreciably to the mean density in these profiles owing to their low number concentration.) The average density displays minimum values of about 400 kg m^{-3} near the cloud top in the updraught and SCR, because of the low-density growth of primary crystals in the dendritic regime above 3.9 km (-12°C). At levels near the base of the sector plate regime between 3.4 and 3.9 km (-9 to -12°C) of the SCR, the average density of primary ice displays a peak value of almost 450 kg m^{-3} . During further descent in the SCR, there is a tendency for their bulk density to be reduced by accretion towards that of rime or accreted ice. Copious young H-M columns cause the total average bulk density of ice to be about 700 to 800 kg m^{-3} within the columnar regime between 2.6 and 3.4 km (-4 to -9°C) in the updraught and SCR of the model cloud. During growth, the H-M columns tend to develop hollow airspaces at their ends and accretion eventually begins in the model. Consequently, their predicted bulk density decreases with decreasing altitude in the SCR towards the freezing level. These predicted values for the density of dendrites, sector-plates and columns during riming are consistent with empirical data (see Heymsfield 1972; Bader *et al.* 1987; Pruppacher and Klett 1997).

Figure 8 depicts the time-averaged profiles of mean AR for ice crystals in the model. A clear tendency for H-M splinters to be columnar ($AR > 1$) in and near the H-M region is evident. H-M columns display a predicted value for AR that exceeds 4:1 near the centre (-5°C) of the H-M region in the updraught, due to growth in the needle regime (-4 to -6°C). This predicted ratio (and the corresponding particle size) is adequately predicted in comparison with the 2D-C images measured by the C-130 aircraft close to the sides of convective turrets at this level (see Hogan *et al.* 2002). Mostly, individual H-M splinters remain columnar for their entire lifetimes. In the SCR, a predicted peak value of average $AR > 4$ of more than four in the needle regime for H-M columns is found to coincide with a peak in the modelled value of observed Z_{DR} of about 0.6 dB (compare Figs. 3 and 8(b) above). This peak value of Z_{DR} is less intense than the intrinsic value of about 4 dB expected for a monodisperse distribution of columns of such high AR , due to the masking effect from a few large H-M particles. During the descent of primary crystals from cloud top in the SCR, rates of accretional growth intensify; columnar

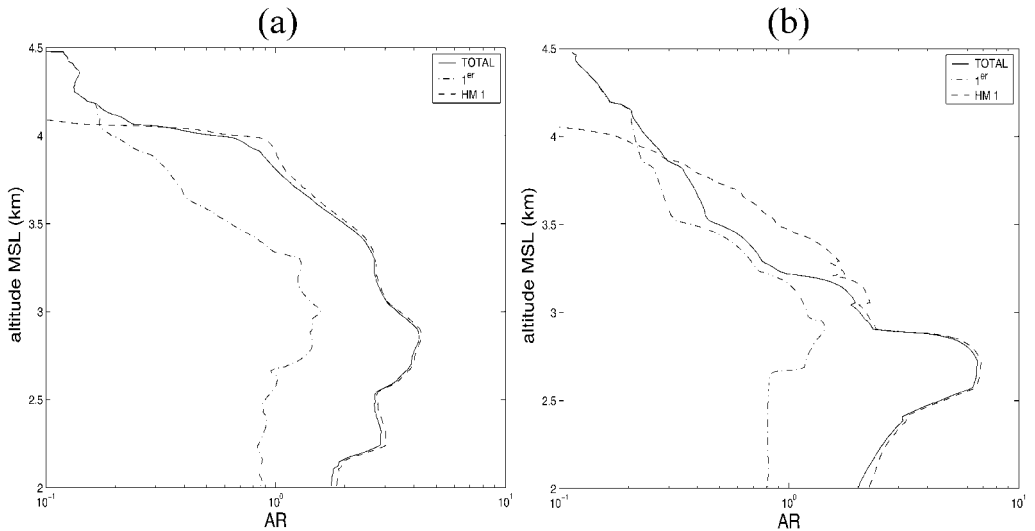


Figure 8. Same as Fig. 6 but for the mean axial ratio (defined in section 2) of ice particles.

regimes are entered. Consequently, AR for primary ice generally tends to increase from 0.1 for dendrites near cloud top towards unity with decreasing altitude. This trend in AR is linked to the trend for the total average Z_{DR} to decline with decreasing altitude.

5. NUMERICAL RESULTS FROM SENSITIVITY TESTS

(a) Ice nucleus (IN) concentration

Three simulations (high-, low- and ultra-low-IN cases) were performed with IN concentrations that were 10, 0.1 and 0.01 times the control value, respectively, at all levels. These runs were compared with the control simulation.

Figure 9 shows that in the high-IN case the average number concentration of H-M splinters is reduced by at least an order of magnitude at most sub-zero levels in the updraught and SCR, relative to the control; also the peak value of the average number concentration of H-M splinters is about an order of magnitude lower than the primary ice number concentration near cloud top. Hence, the average total number concentration of ice particles is reduced by up to about half an order of magnitude in the H-M region of the updraught and by about 20% in the SCR, in the high-IN case relative to the control. There are no intense peaks in total ice number concentration associated with the H-M process anywhere in the model cloud of the high-IN case. In the SCR above the H-M region, the average total number concentration of ice particles is augmented by one order of magnitude in the high-IN case since there are higher number concentrations of primary crystals relative to the control.

The total ice-water content was found to be augmented by about 50% at most levels in the updraught and SCR in the high-IN case; the growth of extra primary ice particles boosts the total mass of ice in the cloud relative to the control. The mean ice diameter is about 0.1 and 0.2 mm higher in the updraught and SCR, respectively, in the high-IN case relative to the control, at sub-zero levels where H-M splinters dominate the total ice number concentration in the control. Enhancement of rates of crystal growth occurs because of the reduced competition for available vapour and reduced evaporation of cloud-water associated with the suppression of the H-M process in the high-IN case.

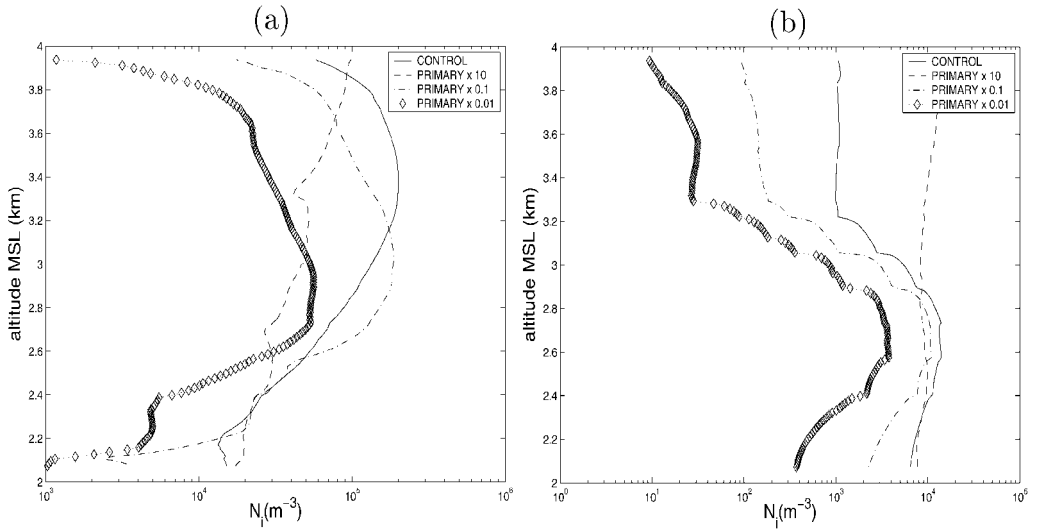


Figure 9. The ice number concentration in: (a) the updraught, and (b) the surrounding cloudy region (SCR), for the high ice-nucleus concentration (high-IN; dashed line), control (full line), low-IN (dot-dashed line) and ultra-low-IN (line with diamonds) cases. See text for details.

However, in the low-IN and ultra-low-IN cases also, the H-M process is less active overall in the model cloud than in the control. This is due to the paucity of rime splintering primary crystals. The average number concentration of H-M splinters is lower by half and one order of magnitude, respectively, in these two cases, at all levels in the SCR and above the H-M region in the updraught, relative to the control. Nonetheless, the higher average droplet size tends to promote the efficacy of the rime splintering process in both cases. Consequently, any generation of H-M splinters in the updraught tends to occur lower in the H-M region relative to the control, at levels where the ascent is fairly weak. Young H-M splinters are then less likely to be upwelled in the updraught aloft than in the control. This accounts for the ice concentration in the lower half of the H-M region of the updraught being more similar to the control value in both cases than at upper levels. There is a reduction of the ice-water content in the SCR by about 50% and 90%, respectively, for both the low- and the ultra-low-IN cases.

Figure 10 shows that the average rate of surface precipitation is 32% higher in the high-IN case than in the control, because a greater fraction of the supply of vapour and cloud-water is converted to primary ice by the Bergeron–Findeisen process and by riming. The average rates of precipitation in the low-IN and ultra-low-IN cases are 24% and 66% lower, respectively. Overall, there is a consistent trend for the average precipitation rate to increase with increasing IN concentration, which matches the parallel trend in the total ice-water content of the SCR.

The cloud-water content aloft is reduced practically to zero over the highest 2 km below cloud top in the SCR, and highest 0.5–1 km of the updraught, in the high-IN case. The peak in cloud-water content near cloud top seen in the control simulation is not present in the high-IN case. Throughout the H-M region, the cloud-water content is reduced by about 40 to 80% in the updraught and to almost zero in the SCR. Furthermore, the mean droplet diameter is reduced by about 2 to 5 microns throughout the H-M region in the updraught of the high-IN case, to values <20 microns. In the

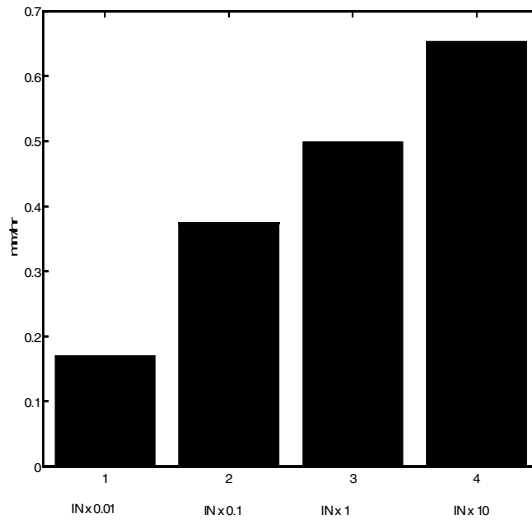


Figure 10. The predicted average rates of surface precipitation for the ultra-low ice-nucleus concentration (IN), low-IN, control, and high-IN cases (left to right). See text for details.

low-IN and ultra-low-IN cases, the cloud-water content is augmented by about 100% and 150%, respectively, at most levels in the model cloud relative to the control, and the peak at cloud top is absent. Also, the average droplet-size is about 5 to 10 μm higher in the low-IN and ultra-low-IN cases at most levels in the model cloud.

Such radical changes in the cloud-water field are explicable in terms of an enhanced Bergeron–Findeisen process caused by deposition of vapour onto higher numbers of primary crystals (and onto their splinter progeny) when the IN concentration is increased. Ice exposes a much higher surface area for vapour deposition when the ice number concentration is higher. Levels near cloud top (-15°C) are close to the optimum temperature for growth of crystals by vapour deposition at water saturation. This is reflected in the response of the cloud-water field being most pronounced at upper levels.

Consequently, the notable suppression of H-M splinter production in the high-IN case is attributed to: (i) the droplet-size dependence of the H-M process and the reduced average size of droplets relative to the control; and (ii) reduced rates of riming by large ice particles due to evaporation of cloud-water. Finally, average values of the total Z_{DR} are enhanced by about 1 to 2 dB at all sub-zero levels in the SCR and by 0.5 to 2 dB in the highest 1 km of the updraught, in the high-IN case relative to the control. This enhancement occurs partly because reduced rates of riming by the largest ice particles allow AR to deviate further from unity, relative to the control. Additionally, reduced rates of accretion increase the average density of ice by about 100–200 kg m^{-3} at most sub-zero levels relative to the control. The radar-reflectivity factor is boosted by a few dB(Z) in the updraught of the high-IN case relative to the control, indicating that higher values of the primary ice number concentration act to favour the formation of large aggregates. In the low-IN case, the Z_{DR} is reduced to values <0.1 dB throughout most of the SCR because the higher cloud-water content promotes higher rates of riming by the largest primary ice particles, rendering these particles more nearly spherical relative to the control.

(b) Cloud condensation nuclei (CCN) concentration

Runs with values of C of 15 and 1500 cm^{-3} in the CCN activity spectrum (the 'ultra-maritime' and 'continental' cases) were compared with the control ($C = 150 \text{ cm}^{-3}$).

The average value of the total ice number concentration was found to be reduced by almost one order of magnitude at most sub-zero levels above the centre of the H-M region in the updraught, and below this level in the SCR, in the continental case. This reduction is caused by reduced rates of H-M splinter production relative to the control. Peak values of the average number concentration of H-M splinters, above and below the centre of the H-M region in the updraught and SCR, respectively, are only about half an order of magnitude greater than the primary ice number concentration near cloud top in the continental case. The total ice-water content is reduced by about 30% at most sub-zero levels in the updraught and by about 5% to 10% below the H-M region in the SCR in the continental case because of the reduced activity of the H-M process relative to the control. A slight increase in the ice-water content by about 0.01 g m^{-3} was found at levels in the SCR above the centre of the H-M region owing to faster growth of primary ice crystals in the continental case. This appears to reflect the presence aloft of a higher supersaturation with respect to ice relative to the control. The average rate of surface precipitation is diminished by about 5% when C is increased beyond the control value.

In the ultra-maritime case, the total ice number concentration is very similar to the control value at all levels. The only appreciable difference is found near the centre of the H-M region of the updraught, where there is a slight increase of the ice number concentration by <10%. This modest change occurs partly because the higher average droplet size directly promotes the H-M process, despite a reduction of about 0.05 g kg^{-1} in the cloud-water content relative to the control. No dramatic changes are found in the total ice-water content. The average rate of precipitation is reduced by about 5% in the ultra-maritime case relative to the control.

The average cloud-water content is augmented by about 50% at certain levels in the continental case relative to the control, where the total ice number concentration is reduced in the updraught and SCR. This is related to the diminished effectiveness of the Bergeron–Findeisen process for vapour growth of ice. The mean droplet diameter is lower by about 5 to 10 microns in the H-M region of the updraught and SCR, displaying values <15 microns, because of higher number concentrations of droplets. Thus, the diminution of H-M splinter production is explicable in terms of the droplet-size dependence of the H-M process in this particular sensitivity test.

As in the high-IN case, there is an enhancement of the Z_{DR} profile aloft in the SCR in the continental case, because the reduced size of droplets lowers the collision efficiency for riming relative to the control. Consequently, lower rates of riming growth of planar primary crystals appear to halve the average axial ratio above the H-M region of the SCR in the continental case relative to the control. This accounts for the intensification of Z_{DR} in the SCR by up to about 1 dB at upper levels in this case.

(c) Vertical shear

In order to examine the dependence of the cloud glaciation on the environmental vertical shear of the horizontal wind, a run was performed with a reduced vertical shear of $0.5 \text{ m s}^{-1} \text{ km}^{-1}$ (the 'low-shear' case). This simulation was compared with the control, in which a vertical shear of $5 \text{ m s}^{-1} \text{ km}^{-1}$ had been applied. The updraught was more nearly vertical in the low-shear case.

Above the H-M region in the updraught, the average number concentration of H-M splinters is about 50% lower in the low-shear case relative to the control. The peak in average total ice number concentration is reduced by 100 l^{-1} in the updraught at 3.2 km altitude. The primary ice number concentration is boosted by $0.1\text{--}0.5 \text{ l}^{-1}$ at most sub-zero levels relative to the control. In the low-shear case, the residence-time of primary crystals in the updraught appears to be prolonged. For example, the reduced slope of the updraught may allow large primary ice particles to fall through the base of one thermal into the next rising thermal. Higher number concentrations of primary ice are associated with a reduction of the cloud-water content in the updraught, presumably by promoting evaporation. This reduces slightly the activity of the H-M process. Notably, the peak in cloud-water content near cloud-top found in the control is diminished by about 20% in the updraught of the low-shear case.

The total ice-water content in the updraught is increased by about 10% due to extra primary ice at most sub-zero levels. It is reduced slightly in the SCR by a few percent between 3 and 4 km owing to the relative paucity of H-M splinters. The average precipitation rate is reduced by about 2% in this particular low-shear case. The Z_{DR} in the SCR is reduced by 0.1 to 0.2 dB at most sub-zero levels in the low-shear case, due to lower primary ice number concentrations and increased riming rates relative to the control. In view of the limited degree of sensitivity found in this particular test, no further perturbation simulations were conducted with respect to the vertical shear.

6. DISCUSSION AND CONCLUSIONS

The forte of the EMM is the detailed representation of the evolution of crystal properties as particles grow from a pristine state into either graupel, snow or rimed aggregates. This representation is possible because the trajectories of individual particles spanning a spectrum of sizes are traced through the cloud. In particular, the explicit prediction of the evolution of the axial ratio along each particle's trajectory allows the differential reflectivity—a function of both particle shape and bulk density—to be predicted.

Adequate agreement was generally found in the stratiform cloud case between the EMM control simulation and observations of the stratiform cloud case by radar and aircraft (see section 4). The predicted properties of ice particles are explicable in terms of: (i) the sequence of temperature-dependent habits for vapour depositional growth encountered by individual particles; and (ii) their history of growth by accretion and riming. Predicted values for the crystal properties of bulk density and axial ratio are consistent with results from laboratory studies summarized by Pruppacher and Klett (1997). The instantaneous maximum value of the ice number concentration near the centre of the H-M region is correctly predicted to be between two and three orders of magnitude higher than the primary ice number concentration near cloud top. The time-averaged total ice number concentration displays a maximum average value of 200 l^{-1} at this level in the EMM control, which is of the correct order of magnitude. Thermals are predicted to be radar-visible as ascending maxima and minima of Z_{H} and Z_{DR} respectively, as is seen in the polarization-diversity radar observations.

Naturally, the agreement between microphysical predictions and observations is not expected a priori to be quantitatively exact in all respects. It suffices to predict correctly the order of magnitude for quantities such as the concentration of a microphysical species. Firstly, standard literature values have necessarily been applied in attempts to estimate the order of magnitude of the concentrations of CCN and IN. Additionally, the updraught strength at cloud base was not observed on this day. The value of vertical air

velocity in the SCR is so close to zero that only its order of magnitude may be inferred from the aircraft observations. Furthermore, a high value of the vertical wind shear was measured in the environment for this case. The physical dependencies of thermal entrainment on the shear and stratification of the ambient fluid appear not to have been fully quantified in laboratory studies in the literature. Hence, it appears that only the order of magnitude of β_E in the real cloud may be inferred reliably from laboratory data. Secondly, multiplicative processes and positive feedbacks are expected to be present in a complex web of microphysical interactions occurring within real mixed-phase cloud.

The peak in average ice number concentration seen near the centre of the H-M region in aircraft observations of the Chilbolton case is accounted for by the detailed representation of the H-M process in the EMM control simulation. Similarly, a peak of the ice concentration in the H-M region was seen in aircraft observations by Bower *et al.* (1996). Overall, the H-M process in the EMM control simulation was found to be more active in thermals than in the SCR due to a higher cloud-water content supported by the more rapid ascent. The hypotheses that slow falling snowflakes may produce H-M splinters and that coalescence is not the major mechanism for precipitation formation in this particular cloud (see sections 2 and 3(a)) appear to have produced a satisfactory control simulation.

Mason (1996) suggested that a different peak in ice concentration observed by Bower *et al.* (1996) at the -15°C level was caused by the accumulation of H-M splinters near the cloud top following their formation in the H-M region. The present study shows that Mason's hypothesis is at least plausible, although no such peak is predicted in the particular cloud simulated in the EMM control. In the dynamical framework of this particular simulation, H-M splinters ascend and then fall out of thermals before the cloud top is attained. Fragmentation of fragile dendritic crystals—either mechanically or during sublimation—seems difficult to eliminate as a possible alternative explanation for the peak at -15°C observed by Bower *et al.* (1996).

Although the H-M process determined the total ice concentration throughout much of the updraught and SCR, primary ice was found to dominate the simulated radar properties of the model cloud. Realistically high values of Z_{DR} of up to almost 4 dB were predicted by the EMM near the cloud top in the SCR of the control simulation. This peak was caused by primary crystals growing in the dendritic (planar) regime by vapour deposition in the model. Such crystals are highly non-spherical. Similarly, high values of Z_{DR} of up to 4 dB were observed near the cloud top level, and were attributed to large dendritic crystals in observations of another case of precipitating stratiform cloud by Bader *et al.* (1987). The accumulation of supercooled cloud-water in the highest 200 m just below the cloud top in the EMM control simulation is typical of supercooled layers reported in observational studies of stratiform cloud. Such cloud-water aloft promotes the dendritic growth of crystals by vapour deposition in the simulation by maintaining water saturation.

Individual slanted regions of high total $Z_{DR} > 1$ dB are sometimes seen extending within the supersaturated environment towards the freezing level near turrets in radar observations of the real cloud (Hogan *et al.* 2002, their Fig. 5). Such high- Z_{DR} regions are observed within only a limited fraction of the total volume of SCR and appear to be transient features. They are seen in the radar data partly because small H-M columns of high intrinsic Z_{DR} can avoid depletion by aggregation within gaps in the 3D fallout of large aggregates. Also, such gaps in the real cloud might tend to 'unmask' temporarily the intrinsic high- Z_{DR} signal from any small crystals such as H-M splinters that are present. The regions of high total Z_{DR} seen in the radar observations are not resolved in the SCR of the EMM control; the EMM treats the SCR as a 1D channel,

and does not directly simulate in 3D the inhomogeneous turbulent flow of the real cloud. Nevertheless, the hypothesis by Hogan *et al.* (2002) that high- Z_{DR} features in the centre of the cloud may be caused by H-M splinters is qualitatively consistent with the model results. The EMM predicts fallstreaks of intrinsic Z_{DR} from H-M splinters with instantaneous values of up to about 2 dB in the H-M region of the supersaturated environment. H-M splinters are present in much of the SCR and almost all of the updraught in the control simulation. Their number concentrations are orders of magnitude higher than the primary ice concentration.

In summary, the EMM sensitivity studies (see section 5) generally indicate that the number concentration of aerosol particles in the environment has a major impact on the glaciation of the frontal cloud. Increasing the concentration of either IN or CCN beyond control values acts to restrict the growth rates of droplets, diminishing the efficacy of the H-M process. Similarly, in previous EMM simulations of deep cumuli by Phillips (2001) and Phillips *et al.* (2001, 2002) the CCN concentration was found to determine whether the droplet-size-dependent H-M process is activated. In the present study, the total ice-water content is reduced by lower rates of H-M splinter production in the continental case relative to the control; the suppression of the H-M process is more than counteracted by the growth of extra primary ice in the response of the ice-water content when IN concentrations are augmented. Also, the precipitation rate below the cloud is found to increase markedly with the atmospheric IN concentration beyond the control value. Naturally, at low IN concentrations there is a point where decreasing the IN concentration below the control value begins to decrease the activity of the H-M process, because of the paucity of particles of primary ice available for rime splintering. The IN concentration appears to be an important quantity that needs to be measured accurately in future campaigns of *in situ* observations.

A key conclusion from the CCN and IN tests described here is that the liquid- and ice-water paths are significantly sensitive in the SCR to the environmental aerosol concentration. Furthermore, the peak in cloud-water content found near cloud top in the control simulation is completely eliminated by extra deposition of vapour onto ice when the IN concentration is increased by an order of magnitude. The total number concentration and mean diameter of ice are similarly sensitive to nucleus concentrations at upper levels. The cloud albedo and emissivity would be affected by such changes in particle number concentration, effective particle size and water path for ice and cloud-water. In particular, the cloud albedo would be expected to be highly dependent on the intensity of the IN-sensitive peak in cloud-water content predicted near cloud top in the EMM control simulation. A major contribution to the global radiation budget comes from spatially extensive SCR regions of stratiform cloud. The appreciable sensitivity of mixed-phase microphysics in EMM simulations of frontal cloud is clearly of paramount importance for the cloud property feedback in global climate change.

ACKNOWLEDGEMENTS

The Natural Environment Research Council as part of the Clouds Water Vapour and Climate Thematic Programme, and the Met Office supported this work. T. J. Phillips, was also at the Geophysical Fluid Dynamics Laboratory (GFDL)/National Oceanic Atmospheric Administration (NOAA), Princeton University, Princeton, USA.

REFERENCES

- Al-Naimi, R. and Saunders, C. P. R. 1985 Measurements of natural deposition and condensation-freezing ice nuclei with a continuous flow chamber. *Atmos. Environ.*, **19**, 1871–1882

- Bader, M. J., Clough, S. A. and Fox, G. P. 1987 Aircraft and dual-polarization radar observations of hydrometeors in light stratiform precipitation. *Q. J. R. Meteorol. Soc.*, **113**, 491–516
- Blyth, A. M. and Latham, J. 1997 A multi-thermal model of cumulus glaciation via the Hallett–Mossop process. *Q. J. R. Meteorol. Soc.*, **123**, 1185–1198
- Bower, K. N., Moss, S. J., Johnson, D. W., Choullarton, T. W., Latham, J., Brown, P. R. A., Blyth, A. M. and Cardwell, J. 1996 A parametrization of the ice-water content observed in frontal and convective clouds. *Q. J. R. Meteorol. Soc.*, **122**, 1815–1844
- Gardiner, B. A. and Hallett, J. 1985 Degradation of in-cloud forward scattering spectrometer probe measurements in the presence of ice particles. *J. Atmos. Sci.*, **2**, 171–180
- Hallett, J. and Mossop, S. C. 1974 Production of secondary ice particles during the riming process. *Nature*, **249**, 26–28
- Heymsfield, A. K. 1972 Ice crystal terminal velocities. *J. Atmos. Sci.*, **29**, 1348–1357
- Hogan, R. J., Field, P. R., Illingworth, A. J., Cotton, R. J. and Choullarton, T. W. 2002 Properties of embedded convection in warm-frontal mixed-phase cloud from aircraft and polarimetric radar. *Q. J. R. Meteorol. Soc.*, **128**, 451–476
- Hoppel, W. A., Fitzgerald, J. W., Frick, G. M., Larson, R. E. and Mack, E. J. 1990 Aerosol size distributions and optical properties found in the marine boundary layer over the Atlantic. *J. Geophys. Res.*, **95**, D4, 3659–3686
- Hussain, K. and Saunders, C. P. R. 1984 Ice nucleus measurement with a continuous-flow chamber. *Q. J. R. Meteorol. Soc.*, **110**, 75–84
- Levine, J. 1959 Spherical vortex theory of bubble-like motion in cumulus clouds. *J. Meteorol.*, **14**, 653–662
- Mason, B. J. 1996 The production of high ice-crystal concentrations in stratiform clouds. *Q. J. R. Meteorol. Soc.*, **122**, 353–356
- Meyers, M. P., DeMott, P. J. and Cotton, W. R. 1992 New primary ice-nucleation parametrizations in an explicit cloud model. *J. Appl. Meteorol.*, **31**, 708–720
- Mitchell, D. 1988 Evolution of snow-size spectra in cyclonic storms. Part I: snow growth by vapour deposition and aggregation. *J. Atmos. Sci.*, **45**, 3431–3451
- Murakami, M. 1990 Numerical modeling of dynamical and microphysical evolution of an isolated convective cloud. *J. Meteorol. Soc. Jpn.*, **68**, 107–128
- Phillips, V. T. J. 2001 ‘Simulations of the glaciation of a New Mexican storm cloud with an explicit microphysics model (EMM)’. PhD Thesis, University of Manchester Institute of Science and Technology, Manchester
- Phillips, V. T. J., Blyth, A. M., Brown, P. R. A., Choullarton, T. W. and Latham, J. 2001 The glaciation of a cumulus cloud over New Mexico. *Q. J. R. Meteorol. Soc.*, **127**, 1513–1534
- Phillips, V. T. J., Choullarton, T. W., Blyth, A. M. and Latham, J. 2002 The influence of aerosol concentrations on the glaciation and precipitation of a cumulus cloud. *Q. J. R. Meteorol. Soc.*, **128**, 951–971
- Pruppacher, H. R. and Klett, J. D. 1997 *Microphysics of clouds and precipitation*. Kluwer Academic Publishers, Dordrecht, the Netherlands
- Reisner, J., Rasmussen, R. M. and Bruintjes, R. T. 1998 Explicit forecasting of supercooled liquid water in winter storms using the MM5 mesoscale model. *Q. J. R. Meteorol. Soc.*, **124**, 1071–1107
- Rogers, R. R. and Yau, M. K. 1991 *A short course in cloud physics*. Pergamon Press, Amsterdam, the Netherlands
- Ryzhkov, A. V., Zrníc, D. S. and Gordon, B. A. 1998 Polarimetric method for ice water content determination. *J. Appl. Meteorol.*, **37**, 125–134
- Sanchez, O., Raymond, D. J., Libersky, L., and Petschek, A. G. 1989 The development of thermals from rest. *J. Atmos. Sci.*, **46**, 2280–2292
- Saunders, C. P. R. and Hosseini, A. S. 2000 ‘A laboratory study of the effect of velocity on Hallett–Mossop ice crystal multiplication’. Pp. 617–620 in Proceedings of the 13th international conference on clouds and precipitation, Reno, Nevada. American Meteorological Society, Boston, USA
- Schnell, R. C., Wrobel, B. and Miller, S. W. 1980 ‘Seasonal changes and terrestrial sources of atmospheric ice nuclei at Boulder, Colorado’. Pp. 53–56 in Proceedings of the cloud physics conference, Clermont-Ferrand. International Commission on Clouds and Precipitation